Computational and Structural Biotechnology Journal 23 (2024) 2453–2464

Contents lists available at ScienceDirect

Computational and Structural Biotechnology Journal

journal homepage: www.elsevier.com/locate/csbj

Short Communication

Reversing the relative time courses of the peptide bond reaction with oligopeptides of different lengths and charged amino acid distributions in the ribosome exit tunnel

Marc Joiret [a,*], Frederic Kerff [b], Francesca Rapino [c], Pierre Close [c], Liesbet Geris [a,d,e]

[a] Biomechanics Research Unit, GIGA In Silico Medicine, Liège University, CHU-B34(+5) 1 Avenue de l'Hôpital, 4000 Liège, Belgium
[b] UR InBios Centre d'Ingénierie des Protéines, Liège University, Bât B6a, Allée du 6 Août, 19, B-4000 Liège, Belgium
[c] Cancer Signaling, GIGA Stem Cells, Liège University, CHU-B34(+2) 1 Avenue de l'Hôpital, B-4000 Liège, Belgium
[d] Skeletal Biology & Engineering Research Center, KU Leuven, ON I Herestraat 49 - Box 813, 3000 Leuven, Belgium
[e] Biomechanics Section, KU Leuven, Celestijnenlaan 300C - Box 2419, B-3001 Heverlee, Belgium

ABSTRACT

The kinetics of the protein elongation cycle by the ribosome depends on intertwined factors. One of these factors is the electrostatic interaction of the nascent protein with the ribosome exit tunnel. In this computational biology theoretical study, we focus on the rate of the peptide bond formation and its dependence on the ribosome exit tunnel electrostatic potential profile. We quantitatively predict how oligopeptides of variable lengths can affect the peptide bond formation rate. We applied the Michaelis-Menten model as previously extended to incorporate the mechano-biochemical effects of forces on the rate of reaction at the catalytic site of the ribosome. For a given pair of carboxy-terminal amino acid substrate at the P- and an aminoacyl-tRNA at the A-sites, the relative time courses of the peptide bond formation reaction can be reversed depending on the oligopeptide sequence embedded in the tunnel and their variable lengths from the P-site. The reversal is predicted to occur from a shift in positions of charged amino acids upstream in the oligopeptidyl-tRNA at the P-site. The position shift must be adjusted by clever design of the oligopeptide probes using the electrostatic potential profile along the exit tunnel axial path. These predicted quantitative results bring strong evidence of the importance and relative contribution of the electrostatic interaction of the ribosome exit tunnel with the nascent peptide chain during elongation.

1. Introduction

For more than five decades, attempts to model protein synthesis and mRNA translation from first principles have been pursued extensively [1–4]. Many factors influence translation speeds across a single transcript (mRNA). At least seven important factors have been identified in the literature. These include differences in cognate, near-cognate, and non-cognate tRNA relative abundance [5–7], tRNA enzymatic modifications [8,9], amino acid residues distribution within the nascent-chain embedded inside the ribosome exit tunnel [10–12], mRNA secondary structure [13–15], proline residues at either A or P site of the ribosome [16,17], steric hindrance between contiguous ribosomes translating the same mRNA molecule [18], and the finite resource of the ribosome pool available in the cell [19–21]. The influences of these many contributing elements are intertwined, which complicates a full understanding of the individual factors. A number of knowledge gaps still prevail and controversies are still unresolved [10,11,16]. For instance, one study has argued that the charged residues are the major determinants of ribosomal velocity [12]. Another study described the ribosome exit tunnel as a protein-sensitive channel with gate-latch action. Their authors argued that side chain specific recognition in the ribosome exit tunnel plays an active role in protein elongation regulation and translational folding [22].

At the catalytic center of the ribosome, the enhancement of the rate of peptide bond formation is due to a precise positioning of the two substrates within the active site (peptidyl-tRNA at the P-site and aminoacylated-tRNA at the A-site) and to the very specific electrostatic local environment [23,30]. The catalytic environment results from the dynamic configuration occurring within the large subunit of the ribosome that can accommodate a variety of substrates pair combination. The C-terminal amino acid of the peptidyl-tRNA at the P-site and the amino acid acylated on the tRNA at the A-site (aa-tRNA) can be any of the twenty amino acids. The number of different pairs of substrates is thus 400, which shows a versatility rarely met for a classical protein enzyme. This variety in substrate pairs only explains part of the variance of the peptide formation rates. The distribution of charged amino acids

* Corresponding author.
E-mail address: marc.joiret@uliege.be (M. Joiret).

https://doi.org/10.1016/j.csbj.2024.05.045
Received 15 March 2024; Received in revised form 10 May 2024; Accepted 27 May 2024
Available online 31 May 2024

upstream of the nascent chain also affects the kinetics of the peptide bond formation [24,25]. The peptide bond formation at the peptidyl transferase center (PTC) is an entropically driven process achieved by reducing the mobility of the substrates. This happens through precise positioning of the two substrates with respect to each other. As thoroughly reviewed by Rodnina for prokaryotes [26], there are currently two models for the movement of protons in the active site of the ribosome, both involving a single isolated water molecule, and describing the reaction scheme of the peptide bond formation. According to the first model, a concerted 'eight-membered proton shuttle' involving 2' and 3'−OH on the tRNA ribose sugar of adenine 76 at the P-site explains the proton movement. According to the second model, a proton wire mechanism involving $2' - OH$ of the ribose in adenosine 2451 of the 23S rRNA explains the proton movement. A solvation effect with an isolated single water molecule, near the P-site tRNA A76 ribose sugar at the PTC is involved in the proton shuttle model; or near the orthophosphate between C75 and A76 of the A-site tRNA at the PTC, in the proton wire model [23–25,27–35]. In both models, a nucleophic attack of the amino group of aa-tRNA from the A-site on the carbonyl carbon of the ester bond in the peptidyl-tRNA in the P-site is key in this reaction scheme.

Steric hindrance near the C-terminal end of the peptidyl-tRNA hampers access to the nucleophilic attack of the $\alpha-$ amino group from the aa-tRNA at the A-site to the carbonyl carbon atom in the ester bond with the tRNA at the P-site. During the peptidyl transfer reaction, the α-amino group of aminoacyl-tRNA positioned in the A site of the ribosome nucleophilically attacks the carbonyl carbon at the ester bond of the peptidyl-tRNA in the P site. This transpeptidation results in a peptidyl-tRNA extended by one amino acid in the A site and a deacylated tRNA in the P site [34]. The nucleophilic attack is believed to be facilitated if the peptidyl-group at the P-site is pulled away from the carbonyl group. This would reduce steric hindrance and open access for the nucleophilic attack from the aa-tRNA A-site amino group. The peptide bond formation between the two aminoacylated-tRNAs proceeds 10 million times faster when catalyzed by the ribosome than when uncatalyzed in bulk solution [27]. The ribosome-catalyzed peptide bond formation kinetics has been extensively studied for decades and is known to be affected by the particular context of the upstream amino acid sequence [25].

The theory of kinetics of catalysis relies on the transition state theory that was introduced by Henry Eyring who linked the rate constant of a chemical reaction to the Gibbs free activation energy of the transition state (TS) [37–39]. In this representation, a catalyzer accelerates a (bio)chemical reaction through a significant reduction in the transition Gibbs free energy barrier that the reactants have to overcome [42]. In our previously published work [42], we hypothesized that the physical forces transmitted mainly through the backbone of the peptidyl-tRNA play a role in the reduction of the Gibbs free energy barrier of the transition state. The mechanical work of these physical forces affects the activation Gibbs free energy of the transition state. The modulation of the Gibbs free energy activation barrier changes the reaction rate constant through Eyring's relation [37–39]. Computing the mechanical work requires the knowledge of the profile of the axial forces acting on the backbone of the peptidyl-tRNA and of the displacement that results from the peptide elongation. One of the main contributing forces acting on the nascent peptide chain is due to the electrostatic interaction arising from the negative electrostatic potential [40,41]. The negative electrostatic potential is caused by the presence of the large number of phosphates moieties lining the inner wall of the ribosome exit tunnel [36] and also the inner surface cavity around the PTC, mainly composed of rRNA. The electrostatic environment exerts forces on the 4 amino acids that are naturally charged in physiological conditions, namely arginine R, lysine K, glutamate E, and aspartate D. These charged amino acids are occasionally incorporated into the peptide nascent chain as determined by their DNA sequence.

Measuring the kinetics of the elongation cycle of the ribosome at codon resolution is a difficult task. Even more experimentally difficult is to split the time course measurement of the cycle into its main substeps: (i) tRNA accommodation and codon-anticodon proofreading at the A site ($k \simeq 0.010\,\mathrm{ms}^{-1}$ in *E.coli*); (ii) peptide bond formation between the carboxy-terminal amino acid at the P-site and the aa-tRNA at the A-site ($k \simeq 10\,\mathrm{ms}^{-1}$ in *E.coli*); (iii) ribosome translocation to the next codon and unloaded-tRNA eviction at the E site ($k \simeq 2.5\,\mathrm{ms}^{-1}$ in *E.coli*). The peptide bond formation is normally not the rate limiting step in elongation. Hence, its effect on translational control is limited. This is true in normal condition in most of the cases. However, if, by chance, the primary sequence of the polypeptide chain upstream the P-site entails a 'difficult' distribution in charged amino acid residues embedded in the tunnel, the modulation of the peptide bond formation rate due to the electrostatic interaction with the tunnel could turn this step into a limiting step. Other limiting peptide bond formation well known situations are encountered when consecutive prolines, as donor and acceptor substrates, occupy the P-site and A-site. In practice, studying the catalyzed kinetics of peptide bond formation is possible only when peptidyl transfer is uncoupled from the very first step of elongation, i.e., accommodation of the aminoacyl-tRNA at the A site [27,28]. The reason is that the accommodation rate of aa-tRNA in the A site is in the range $5 - 10\,\mathrm{s}^{-1}$ and peptide bond formation follows instantaneously. Because accommodation precedes peptide bond formation, it limits the rate of product formation since it is much slower than the peptidyl transfer [28].

One way to circumvent the accommodation rate limiting step is to use substrate analogs that bind to the A site rapidly and do not require accommodation. If the full length aa-tRNA is replaced by the shorter puromycin substrate as the last acceptor substrate, the kinetics of the catalytic chemical step can be monitored experimentally by the quench flow technique and is amenable to quantitative measurements [27]. These experimental measurements were conducted on prokaryotic ribosomes by Rodnina and coworkers [24] in the elongation minimal case when the donor substrate is the minimal dipeptidyl-tRNA, i.e. $\mathrm{fMet} - \mathrm{X} - \mathrm{tRNA}$ and the acceptor substrate is puromycin, Pmn. X can be any of the 20 natural amino acids. The product of the catalyzed reaction, peptidyl-puromycin, is released from the ribozyme upon completion of the reaction. The experimental initial condition for the puromycin concentration was 20 mM and the reaction rate constant measurements made at $37\,°C$ were obtained by single exponential fitting [24]. The use of puromycin as the last A-site substrate acceptor allows easier experimental measurements of the time courses of peptide bond formation in a quench-flow apparatus measuring the reaction kinetics. In our earlier works, we made use of the electrostatic local profile in the immediate vicinity of the catalytic center of the ribosome to quantitatively interpret these pioneering experimental results [24,42]. From the electrostatic potential profile, we calculated the axial electric field and axial force acting locally on the charged amino acids. These forces modulate the activation energy of the peptide bond formation reaction. The modulation of the reaction rate constant and the time course of the peptide bond formation were calculated accordingly and compared to the experimental kinetics measurements that were made *in vitro* in cell free extracts [24]. In summary, the peptide bond formation median rate fold change between a charged amino acid donor substrate and puromycin as the acceptor substrate was calculated to be 3.45 as compared to a neutral amino acid donor. The experimentally observed values for the median time courses of peptide bond formation with lysine or arginine as donor substrate were 7.2 ms and 7.8 ms, respectively, to be compared with a median time course of 27.1 ms for neutral amino acids as donor substrate (median time course for alanine, serine, phenylalanine and valine) [24,42]. Interestingly, when aspartate is the donor substrate, the calculated fold change is $\frac{1}{3.45} = 0.29$ to be compared with an experimentally measured median time course of 91.5 ms for aspartate. Overall, aspartate (negatively charged aa) is 3.45 times slower than a neutral amino acid, whereas lysine or arginine (positively charged aa) is 3.45 times faster than a neutral amino acid when acting as donor substrate in the minimal case of a dipeptidyl-tRNA at

the P-site with puromycin as the acceptor substrate at the A-site. The experimental order of magnitude for the fold change on these median time courses is qualitatively and quantitatively in good agreement with the theoretical calculations [42].

Here, we expand our previous work to the cases considering the electrostatic interaction on the nascent oligopeptide chain deeper in the exit tunnel. We investigate the effects of the axial forces originating from a much further region than the catalytic center vicinity. A longer oligopeptide acylated to the tRNA at the P-site (much longer than a dipeptide) would probe the electrostatic interaction deeper in the ribosome exit tunnel. The resulting axial forces would still be transmitted to the carboxy-terminal end of the oligopeptidyl-tRNA through the nascent chain backbone and affect the transition state energy barrier of the peptide bond formation. The profiles of the electrostatic potential and the electric field were determined in the full extent of the ribosome exit tunnel in previous work by ourselves and others [36,40]. Those results are used to compute the axial forces acting on charged amino acids arbitrarily distributed in oligopeptides embedded in the ribosome exit tunnel.

One of the big challenges in the field of translational control and protein elongation is how to address the kinetics of the processes involved. Our approach focused on a well identified step in the protein elongation cycle and provides a quantitative tool to understand the impact of mechanochemical factors on the peptide bond formation rate. The interest of the incorporation of a term accounting for the effect of mechanical forces on the ribosomal catalytic activity and on the equation describing the kinetics is that it allows quantitative estimations of the peptide bond formation rate in different contexts. These quantitative estimations can be confronted with experimental measurements in different settings where some of the above intertwined factors may be adjusted or not. Altogether, these quantitative kinetics approaches will help determine the direct causal links between the factors allegedly affecting, or not, the protein elongation cycle.

2. Materials and methods

This study builds on the model developed in a previous contribution [42]. We briefly recall the key concepts below, before applying them to the case of an elongating nascent polypeptide extending inside the ribosome exit tunnel that is the focus of this study.

2.1. Effect of mechanical forces on chemical reaction kinetics

Applying external forces on molecules involved in catalyzed or uncatalyzed chemical reactions affects the kinetics of the reactions. The mechanical work of these applied mechanical forces can quantitatively be incorporated in the calculation of the activation Gibbs free energy of the transition state as conceptually introduced by Bell [44], Bustamante [45] and others [46]:

$$\Delta G^{\ddagger 0}(\vec{\mathbf{F}}) = \Delta G^{\ddagger 0}(\mathbf{0}) - \int \vec{\mathbf{F}} \cdot \mathbf{d}\vec{\mathbf{x}} \tag{1}$$

where $\Delta G^{\ddagger 0}(\vec{\mathbf{F}})$ is the activation energy for the transition state in the presence of an applied force acting on the system, $\Delta G^{\ddagger 0}(\mathbf{0}) \sim +14\,\mathrm{kcal/mol} = +97.2\,\mathrm{pN\cdot nm}$ is here the activation energy of the deacylation and peptidyl transfer for the transition state without any applied force [25,29,45], and $W = \int \vec{\mathbf{F}} \cdot \mathbf{d}\vec{\mathbf{x}}$ is the mechanical work exerted by the force upon a test body along its curvilinear path. The mechanical work W is algebraically positive if the force and the displacement are parallel or negative if they are antiparallel. In the former case, $\Delta G^{\ddagger 0}(\vec{\mathbf{F}})$ is smaller than $\Delta G^{\ddagger 0}(\mathbf{0})$, whereas it is larger in the latter case. In turn, the modulation of the Gibbs free energy activation barrier changes the reaction rate constant through Eyring's relation [37–39]:

$$k(\vec{\mathbf{F}}) = \kappa \cdot \left(\frac{k_B \cdot T}{h}\right) \cdot e^{-\Delta G^{\ddagger 0}(\vec{\mathbf{F}})/k_B T} \tag{2}$$

$$k(\vec{\mathbf{F}}) = \kappa \cdot \left(\frac{k_B \cdot T}{h}\right) \cdot e^{-\left(\frac{\Delta G^{\ddagger 0}(\mathbf{0})}{k_B T} - \frac{\int \vec{\mathbf{F}} \cdot \mathbf{d}\vec{\mathbf{x}}}{k_B T}\right)} = k(\mathbf{0}) \cdot e^{\frac{\int \vec{\mathbf{F}} \cdot \mathbf{d}\vec{\mathbf{x}}}{k_B T}} \tag{3}$$

where $k(\vec{\mathbf{F}})$ is the reaction rate constant of the rate limiting step in the presence of an applied force upon the substrate at the P-site, $k(\mathbf{0})$ is the reaction rate constant in the absence of applied force. k_B, h and κ are Boltzmann's constant, Planck's constant and transmission coefficient respectively [37–39].

2.2. Modified Michaelis-Menten kinetics

The peptide bond formation kinetics at the catalytic center of the ribosome can be described by the Michaelis-Menten model where the aminoacyl-tRNA (acceptor substrate) is the canonical substrate and where the C-terminal amino acid of the peptidyl-tRNA (donor substrate) behaves as an allosteric substrate [42].

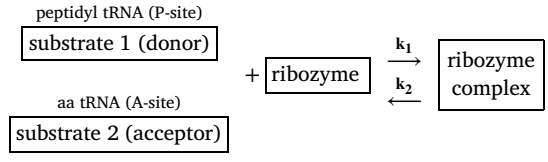

(4)

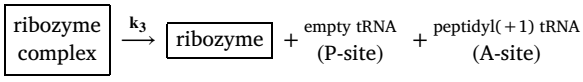

(5)

The rate of peptide bond formation, $k_{\mathrm{pep}} = \frac{dP}{dt}$, is written as follows:

$$\frac{dP}{dt} = \upsilon'_{max} \cdot \frac{S}{K_{1/2} + S} \tag{6}$$

$$\upsilon'_{max} = \frac{\upsilon_{max}}{1 + \frac{S_{allo}}{k_{allo}}} \tag{7}$$

where $K_{1/2} = \frac{k_2 + k_3}{k_1}$ is the Michaelis constant of substrate 2, S, at the A-site; S_{allo} is the C-terminal amino acid at the peptidyl-tRNA (substrate 1); k_{allo} is the reaction rate constant between substrate 1 and the ribozyme (PTC) at the P-site and υ_{max} is the maximum rate in the absence of allosteric effect ($\upsilon_{max} = k_3 \cdot [\mathrm{ribozyme}]$). Incorporating the right hand side Maxwell-Boltzmann factor of (3) into (6) to account for the effect of mechanical forces in the kinetics of the ribozyme catalyzed peptide bond formation leads to the final kinetics equation:

$$\frac{dP}{dt} = e^{\frac{\int \vec{\mathbf{F}} \cdot \mathbf{d}\vec{\mathbf{x}}}{k_B T}} \cdot \upsilon'_{max}(\mathbf{0}) \cdot \frac{S}{K_{1/2} + S} \tag{8}$$

where $\upsilon'_{max}(\mathbf{0})$ is the maximum reaction rate in the absence of external force. In single molecule experiments, P, when proper normalized, represents the probability of the formation of the peptide bond over time in equation (8).

2.2.1. Electrostatic potential and axial forces profile contributed by the catalytic center cavity and by the ribosome exit tunnel

A full closed analytical expression for the electrostatic potential inside the ribosome exit tunnel was proposed earlier which was fitted to the experimental data point measurements of the electrostatic potential obtained by Deutsch and coworkers on ribosomes collected from rabbit reticulocytes [40,41]. More recently, an electrostatic model of the cavity around the catalytic center considering the most simple shape fulfilling the minimal geometrical constraints existing between the ribosome peptide exit tunnel, the mRNA channel and the size of the aminoacylated-tRNAs was developed in [42] leading to the potential profile shown in Fig. 1. The axial force profile allows to determine the mechanical work exerted upon a charged amino acid residue during the peptide elongation process. The method to derive the calculation of the axial forces acting upon any charged residue distribution from the electrostatic potential profile inside the exit tunnel is developed in Joiret et al. [36].

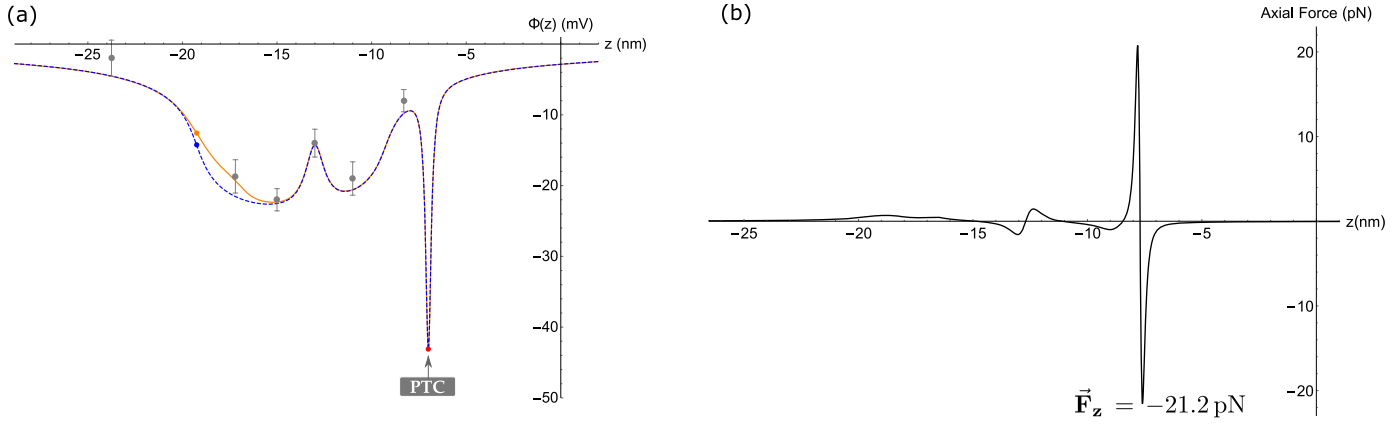

Fig. 1. Electrostatic potential and axial force profiles around the ribosome PTC and the exit tunnel. **(a)** Electrostatic potential profile $\Phi(z)$ as modeled in [36,42]. z is the coordinate along the tunnel center line: $z = -7$ nm is the position of the PTC and $z < -7$ nm is the region through the exit tunnel. The PTC is ∼ 7 nm away from the mRNA decoding center ($z = 0$). The dashed blue line is the potential profile assuming a cylindrical shape at the distal end of the tunnel. Orange line is the potential profile assuming a cone frustum (enlarged tunnel exit). Error bars: experimental data point measurements by Deutsch & coworkers [40] of the potential inside rabbit reticulocytes' ribosome exit tunnel. **(b)** Axial force profile along the z-axis. The axial force $\vec{\mathbf{F}}_z = q_e \cdot \vec{\mathbf{E}}_z$, where $\vec{\mathbf{E}}_z = -\frac{\partial \Phi(z)}{\partial z}$, the electric field along the $z-$ axis, is the negative of the first derivative of the electrostatic potential $\Phi(z)$ profile (shown in **a**). The axial force on a unit positive charge $|q_e|$ at the P-site is $\vec{\mathbf{F}}_z = -21.2$ pN as calculated in reference [42].

2.2.2. Elongation extended case with oligopeptides of variable lengths and puromycin

Building on the above explained framework, here, we study the impact of the electrostatic interaction between the nascent chain and the ribosome exit tunnel on the peptidyl transfer kinetics at the catalytic center. To do that, longer oligopeptides are required as P-site peptidyl-tRNA substrates. The global reaction scheme for the elongation extended case is:

$$\underbrace{\text{fMet-oligoP-X-tRNA}}_{P-site} + \underbrace{\text{(Pmn)}}_{A-site} \rightarrow \underbrace{\text{empty tRNA}}_{P-site} + \underbrace{\text{fMet-oligoP-X-Pmn}}_{A-site} \quad (9)$$

The number of amino acid residues separating the PTC from the ribosome exit tunnel entry point was estimated to be 5 residues from the P-site or 6 residues from the A-site [47]. In what follows, three different oligopeptide lengths are used to probe the effect of the electrostatic interaction inside the ribosome exit tunnel. The oligopeptide lengths are chosen such that they extend inside the beginning of the ribosome exit tunnel and almost up to the tunnel vestibule exit end:

- a 10-mer oligopeptide extended length, with charged residues distributed specifically at position 6, 7, 8 from the C-terminal end of the peptidyl-tRNA at the P-site;
- a 22-mer oligopeptide extended length, with charged residues distributed specifically at position 18, 19, 20;
- a 40-mer oligopeptide extended length, with charged residues distributed specifically at position 35, 36, 37, 38, 39 from the C-terminal end of the peptidyl-tRNA at the P-site.

Except for these locally positioned charged residues, the other amino acid residues are neutral in these oligopeptides.

2.2.3. Output variable uncertainty of the model estimated by differential calculus and uncertainty propagation from the input variables

There are a number of assumptions in the electrostatic model and several sources of uncertainties. These were extensively described and discussed in references [36,42]. The theoretical uncertainty in the peptide bond formation theoretical rate can be estimated from the differential calculus applied to the electrostatic potential model. The numerical errors propagation is detailed in the appendix.

The experimental uncertainties in the peptide bond formation rate k are around $\Delta k \pm 1.5\,\text{sec}^{-1}$ [24]. Given that $\Delta\tau_{1/2} \sim \frac{\Delta k}{k^2}$, it can be estimated that the experimental uncertainties in the median time course measurements are around $1 - 3$ ms.

3. Results

3.1. Axial force profiles and forces transmitted to the carboxy-terminal end of the tRNA at the P-site

These synthetic peptide oligomers sequences were designed such that they are experiencing qualitatively very different electrostatic potential profiles, resulting in different axial forces. In the first case (10-mer), the tunnel electrostatic potential profile in the $z = [-8.9, -9.4]$ nm spatial range will mainly contribute to the axial force transmitted through the backbone of peptidyl-tRNA. In the second case (22-mer), the $z = [-11.95, -12.45]$ nm spatial range will mainly contribute to the axial force. In the last case (40-mer), the $z = [-16.20, -17.20]$ nm spatial range will mainly contribute to the axial force. In the first case, the electrostatic potential is decreasing, whereas in the second and third cases, the potential is increasing toward the tunnel exit direction. The directions of the axial forces being exerted on positively (or negatively) charged test residues are opposite. The qualitative effects on the kinetics of the peptidyl transfer reaction with puromycin at the A-site are expected to be in opposite directions as well. This is the cause of the reversing in the reaction relative time courses.

In the first case, the 10-mer nascent oligopeptide acylated tRNA at the P-site threads through the ribosome tunnel entry (Fig. 2 a-c). The axial force acting upon the backbone of the peptidyl-tRNA and transmitted to the tRNA at the P-site caused by three positively charged residues within the oligopeptide is calculated using the algorithm that was earlier exposed [36] and is $\vec{\mathbf{F}}_z = -2.61$ pN. The mechanical work is estimated to be $W = 2.61\,\text{pN} \cdot 0.25\,\text{nm} = 0.65\,\text{pN} \cdot \text{nm}$ (force and displacement are parallel).

In the second case, the 22-mer nascent oligopeptide acylated tRNA at the P-site threads further through the ribosome tunnel entry (Fig. 3 a-c). Similarly to the previous case, the axial force acting upon the backbone of the peptidyl-tRNA and transmitted to the tRNA at the P-site caused by three positively charged residues within the oligopeptide is $\vec{\mathbf{F}}_z = +3.42$ pN. The mechanical work is estimated to be $W = -3.42\,\text{pN} \cdot 0.25\,\text{nm} = -0.86\,\text{pN} \cdot \text{nm}$ (force and displacement are antiparallel).

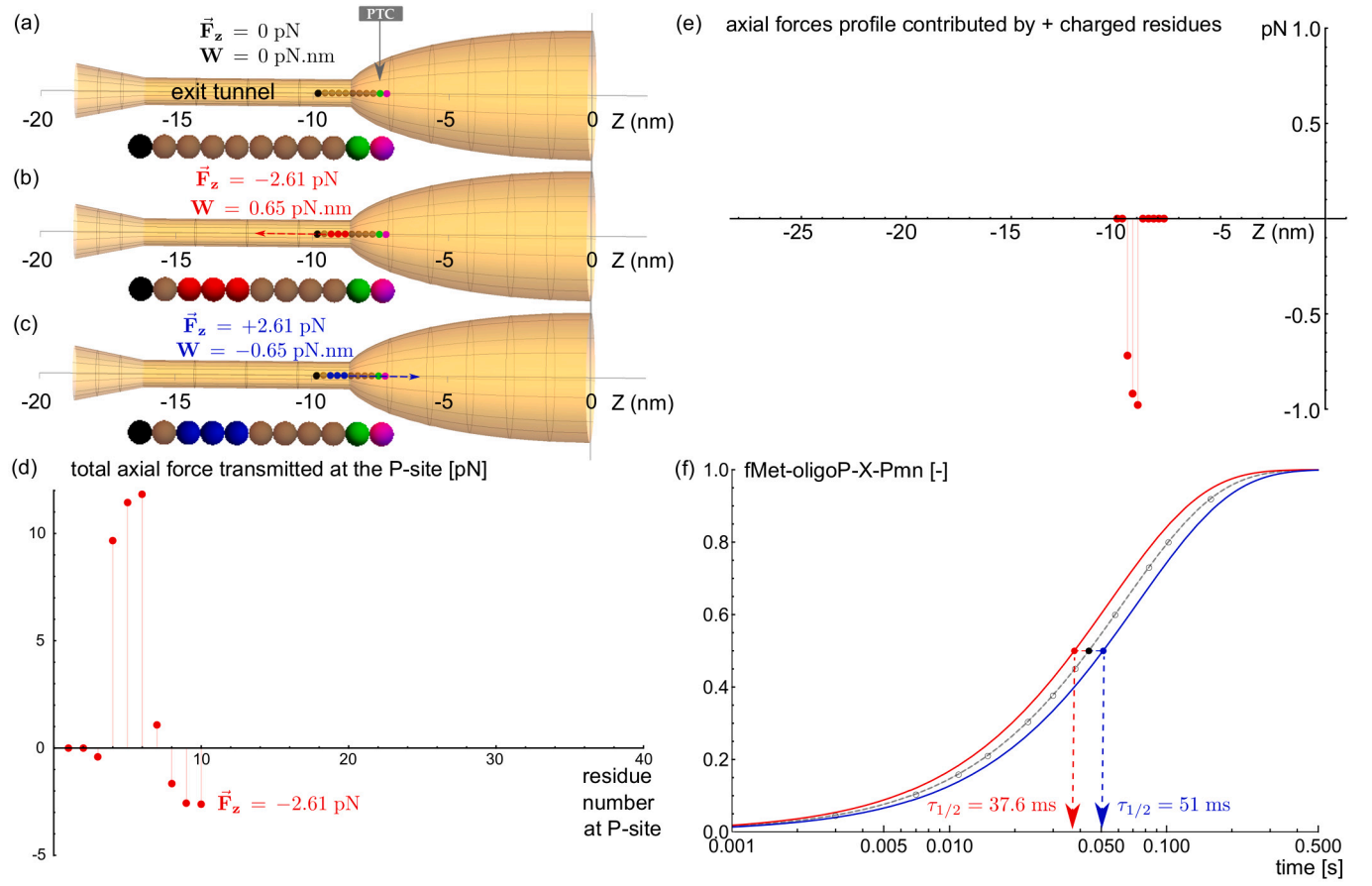

Fig. 2. Elongation extended case: effect of force on the rate of peptide bond formation when the P-substrate is a 10-mer oligopeptidyl-tRNA (fMet-oligoP-X-tRNA). Electrostatic force acting on X at the P site: **(a)** OligoP = Neutral oligo-alanine (brown sphere). **(b)** OligoP = Positively charged amino acid R at position 6, 7, 8 (red sphere). **(c)** OligoP = Negatively charged amino acid D at position 6, 7, 8 (blue sphere). Methionine (black sphere). X = phenylalanine (green sphere). Puromycin (magenta sphere). **(d)** Total axial force acting on the nascent peptide at the last amino acid residue (counted from N-terminal end) occupying the ribosomal PTC position, as calculated from the algorithm in Joiret et al. [36]. **(e)** Axial force profile contributed by positively charged residues when located at indicated z-position from the PTC. **(f)** Predicted normalized time courses of the Pmn (20mM) reaction with different oligopeptidyl-tRNAs: calculated theoretical normalized time courses using Maxwell-Boltzmann factors. Neutral oligoP-Phe(○)($\tau_{1/2} = 43.8$ ms), dashed line. Positively charged amino acid C-terminal oligopeptidyl-transfer rate ($\tau_{1/2} = 37.6$ ms), red line. Negatively charged amino acid oligopeptidyl-transfer rate ($\tau_{1/2} = 51$ ms), blue line.

In the third case, the 40-mer nascent oligopeptide acylated tRNA at the P-site threads deeper through the ribosome tunnel down to the vestibule exit (Fig. 4 a-c). The axial force acting upon the backbone of the peptidyl-tRNA, caused by the five positively charged residues and transmitted to the tRNA at the P-site is $\vec{\mathbf{F}}_z = +2.1$ pN. The mechanical work is estimated to be $W = -2.1\,\text{pN} \cdot 0.25\,\text{nm} = -0.525\,\text{pN} \cdot \text{nm}$ (force and displacement are antiparallel).

3.2. Peptide bond formation reaction rates with 10, 22 and 40-mer oligopeptide and puromycin

We predict the Maxwell-Boltzmann factors and the reaction rate constant values tabulated in Table 1. The predicted time courses of the 10-mer oligopeptidyl-tRNA reaction with Pmn are shown in Fig. 2 (f). The red and blue lines are the time courses calculated from equation (8) for the positively and negatively charged case respectively as compared to the neutral case (dashed line). The positively charged amino acid C-terminal oligopeptidyl-transfer rate is $k(\mathbf{0}) \times \exp(\int \vec{\mathbf{F}} \cdot d\vec{\mathbf{x}}/k_B T) =$ neutral rate $\times \exp(0.65/4.28) =$ neutral rate $\times$ 1.16 (red line). The negatively charged amino acid oligopeptidyl-transfer rate is $k(\mathbf{0}) \times \exp(-0.65/4.28) =$ neutral rate $\times$ 0.86 (blue line). At their specific positions from $z = -8.95$ nm to $z = -9.45$ nm the three positive charged residues pull the oligopeptidyl-tRNA backbone toward the exit tunnel and the peptide bond formation rate is increased as compared to the neutral oligopeptidyl-tRNA. With three negative charged residues, the resulting axial force points in the opposite direction and the peptide bond formation rate is decreased as compared to the neutral case.

3.3. Estimated theoretical uncertainty for the median time course of the peptide bond formation reaction

The theoretical uncertainties in the output variable that are propagated from the electrostatic potential model to the peptide bond formation reaction rate and the median time course theoretical calculation are numerically estimated by differential calculus as detailed in the appendix. Numerical estimates of the uncertainties $\Delta\,\tau_{1/2}^{th.}$ in the median time courses of the peptide bond formation are listed in the last column of Table 1. The upper script th. in $\Delta\,\tau_{1/2}^{th.}$ means it refers to a model dependent theoretical uncertainty.

The predicted time courses of the 22-mer oligopeptidyl-tRNA reaction with Pmn are shown in Fig. 3 (f). At their specific positions from $z = -11.95$ nm to $z = -12.45$ nm the three positive charged residues push the oligopeptidyl-tRNA backbone toward the P-site and the peptide bond formation rate is decreased as compared to the neutral oligopeptidyl-tRNA. With three negative charged residues, the resulting axial force points in the opposite direction and the peptide bond formation rate is increased as compared to the neutral case. This is qualitatively the opposite situation as the one encountered in the previous case with the 10-mer oligopeptide.

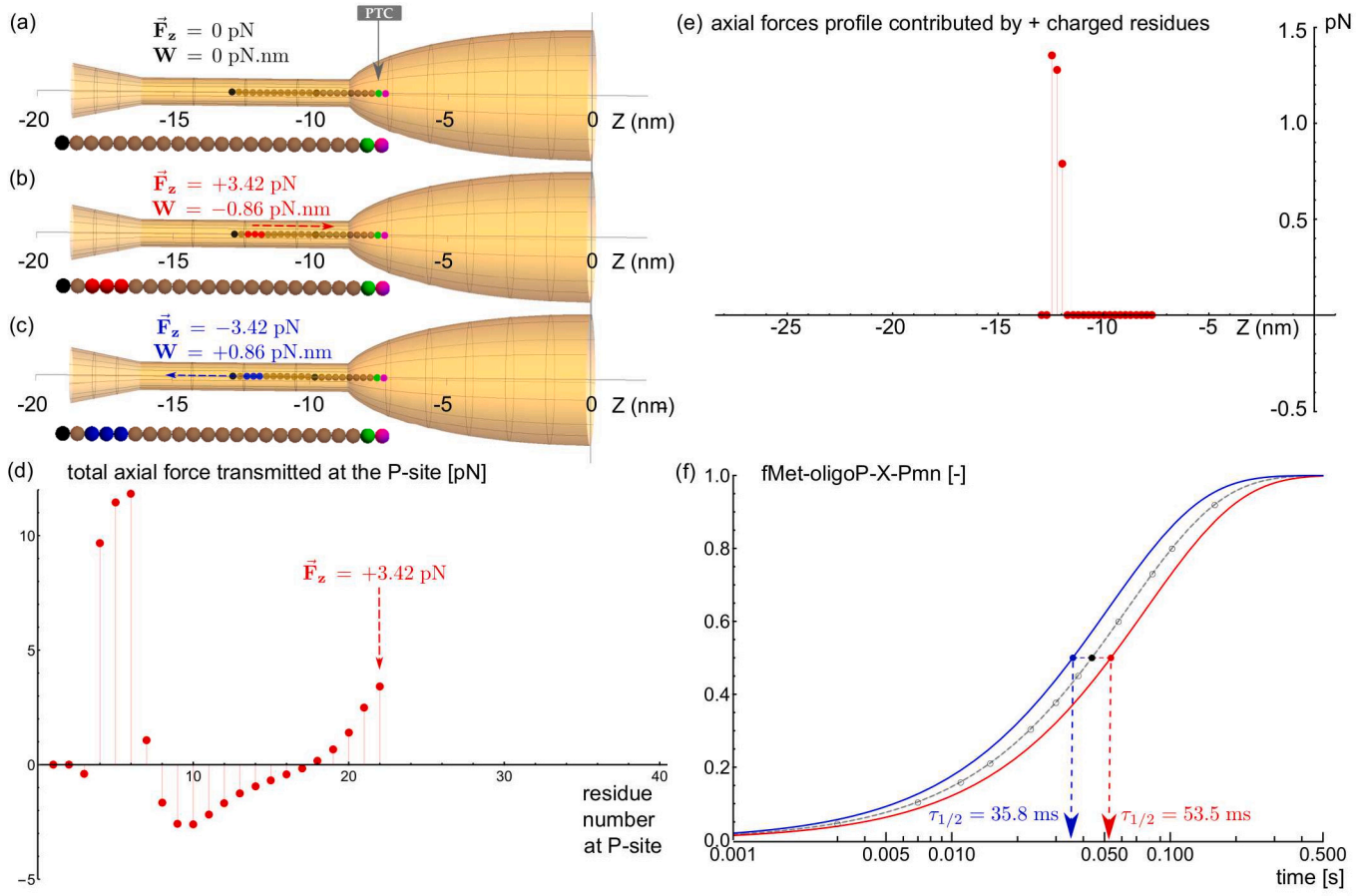

Fig. 3. Elongation extended case: effect of force on the rate of peptide bond formation when the P-substrate is a 22-mer oligopeptidyl-tRNA (fMet-oligoP-X-tRNA). Electrostatic force acting on X at the P site: **(a)** OligoP = Neutral oligo-alanine (brown sphere). **(b)** OligoP = Positively charged amino acid R at position 18, 19, 20 (red sphere). **(c)** OligoP = Negatively charged amino acid D at position 18, 19, 20 (blue sphere). Methionine (black sphere). X = phenylalanine (green sphere). Puromycin (magenta sphere). **(d)** Total axial force acting on the nascent peptide at the last amino acid residue (counted from N-terminal end) occupying the ribosomal PTC position, as calculated from the algorithm in Joiret et al. [36]. **(e)** Axial force profile contributed by positively charged residues when located at indicated z-position from the PTC. **(f)** Predicted normalized time courses of the Pmn (20mM) reaction with different oligopeptidyl-tRNAs: calculated theoretical normalized time courses using Maxwell-Boltzmann factors from equations (3) and (8). Neutral oligoP-Phe(○)($\tau_{1/2} = 43.8$ ms), dashed line. Positively charged amino acid C-terminal oligopeptidyl-transfer rate ($\tau_{1/2} = 53.5$ ms), red line. Negatively charged amino acid oligopeptidyl-transfer rate ($\tau_{1/2} = 35.8$ ms), blue line.

Table 1
Maxwell-Boltzmann factors $\exp(\int \vec{\mathbf{F}} \cdot d\vec{\mathbf{x}}/k_B T)$ modulating the x-mer (x = 10, 22, 40) oligopeptidyl transfer rate constants $k(\vec{\mathbf{F}})$, the waiting time $\tau_{1/2}$ to peptide bond formation event with a probability of 0.5, and theoretical uncertainty on $\tau_{1/2}$. C-terminal residue at P site is phenylalanine. Acceptor substrate at A-site is puromycin. $k(\mathbf{0})$: rate constant in the absence of force (neutral case). fMet: formyl-methionine. Circled dot: neutral; circled plus: positively charged; circled minus: negatively charged oligopeptides respectively, with specific amino acid distributions as detailed in the text.

P-site x-mer oligopeptide with charged residues acting at P-site		Mechanical work (pN.nm)	Maxwell Boltzmann factor (-)	Rate constant $k(\vec{\mathbf{F}})$ (s^{-1})	$\tau_{1/2}$ (ms)	Uncertainty $\Delta\tau^{th.}_{1/2}$ (ms)
10-mer	$fMet \odot -tRNA(0)$	0.0	1	$k(\mathbf{0})$	43.8	
	$fMet \oplus -tRNA(+3)$	+0.65	1.16	$1.16 \cdot k(\mathbf{0})$	37.6	4.3
	$fMet \ominus -tRNA(-3)$	−0.65	0.86	$0.86 \cdot k(\mathbf{0})$	51	5.9
22-mer	$fMet \odot -tRNA(0)$	0.0	1	$k(\mathbf{0})$	43.8	
	$fMet \oplus -tRNA(+3)$	−0.86	0.81	$0.81 \cdot k(\mathbf{0})$	53.5	5.3
	$fMet \ominus -tRNA(-3)$	+0.86	1.22	$1.22 \cdot k(\mathbf{0})$	35.8	3.6
40-mer	$fMet \odot -tRNA(0)$	0.0	1	$k(\mathbf{0})$	43.8	
	$fMet \oplus -tRNA(+5)$	−0.525	0.88	$0.88 \cdot k(\mathbf{0})$	49.5	7
	$fMet \ominus -tRNA(-5)$	+0.525	1.13	$1.13 \cdot k(\mathbf{0})$	38.7	5.4

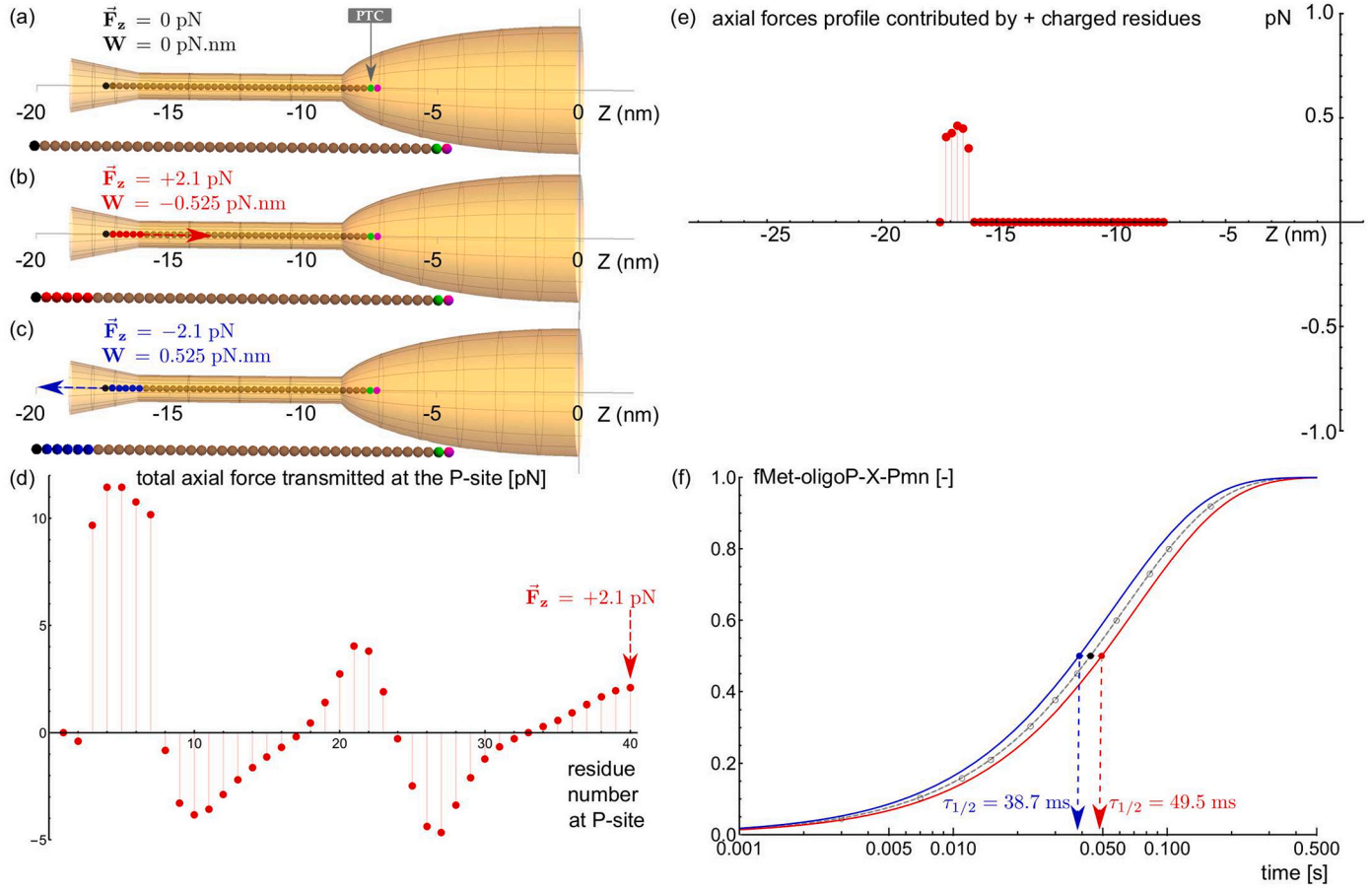

Fig. 4. Elongation extended case: effect of force on the rate of peptide bond formation when the P-substrate is a 40-mer oligopeptidyl-tRNA (fMet-oligoP-X-tRNA). Electrostatic force acting on X at the P site: **(a)** OligoP = Neutral oligo-alanine (brown sphere). **(b)** OligoP = Positively charged amino acid R at position 35, 36, 37, 38, 39 (red sphere). **(c)** OligoP = Negatively charged amino acid D at position 35, 36, 37, 38, 39 (blue sphere). Methionine (black sphere). X = phenylalanine (green sphere). Puromycin (magenta sphere). **(d)** Total axial force acting on the nascent peptide at the last amino acid residue (counted from N-terminal end) occupying the ribosomal PTC position, as calculated from the algorithm in Joiret et al. [36]. **(e)** Axial force profile contributed by positively charged residues when located at indicated z-position from the PTC. **(f)** Predicted normalized time courses of the Pmn (20mM) reaction with different oligopeptidyl-tRNAs: calculated theoretical normalized time courses using Maxwell-Boltzmann factors from equations (3) and (8). Neutral oligoP-Phe(○)($\tau_{1/2} = 43.8$ ms), dashed line. Positively charged amino acid C-terminal oligopeptidyl-transfer rate ($\tau_{1/2} = 49.5$ ms), red line. Negatively charged amino acid oligopeptidyl-transfer rate ($\tau_{1/2} = 38.7$ ms), blue line.

The predicted time courses of the 40-mer oligopeptidyl-tRNA reaction with Pmn are shown in Fig. 4 (f). At their specific positions from $z = -16.2$ nm to $z = -17.20$ nm the five positive charged residues push the oligopeptidyl-tRNA backbone toward the P-site and the peptide bond formation rate is decreased as compared to the neutral oligopeptidyl-tRNA. With the five negative charged residues, the resulting axial force points in the opposite direction toward the exit tunnel and the peptide bond formation rate is increased. This is also qualitatively the opposite situation as the one encountered in the first case with the 10-mer oligopeptide. The interesting new predicted hypothetical result is that it should be possible to observe a reversing in the relative time courses of the peptide bond reaction between the two donor and acceptor amino acids at the P- and A-site with different charged amino acid distributions upstream in the probed oligopeptides. This requires the use of oligopeptidyl-tRNAs of different lengths at the P-site with amino acid sequences for which the nature (+ or -) and the space distribution of charges have been carefully positioned by design.

4. Discussion

In our theoretical study, we incorporated as an additional argument of the Maxwell-Boltzmann factor in the Eyring equation, a term accounting for the effect of mechanical forces on a catalyzed reaction. The work of external electro-mechanical forces can affect the Gibbs free energy barrier of the transition state. A modified Michaelis-Menten model is applied to the kinetics of the ribozyme catalyzing the peptidyl transfer reaction in the large subunit of the ribosome. Our theoretical derivation is quantitatively consistent with the large difference in the time courses of the peptide bond formation that was experimentally observed in the dipeptide minimal case [24] between neutral, positively and negatively charged amino residues positioned at the carboxyl-terminal end of the dipeptidyl-tRNA at the P-site. This confirms that the electrostatic interaction is an important contributing force affecting the transition state barrier for the catalytic reaction taking place at the PTC.

We further predicted that the time courses of the peptide bond formation between a given C-terminal amino acid residue of the peptidyl-tRNA at the P-site with a given aminoacyl-tRNA at the A-site is dependent on the distribution of upstream charged amino acid residues within the peptidyl-tRNA embedded in the exit tunnel. Specifically, depending on whether these charged amino acid residues are positive or negative and are located in the upper tunnel, before or after the tunnel constriction site (where the ribosomal proteins uL4 and uL22 protrude), or in the lower tunnel near the tunnel exit point, the peptide bond formation time courses are predicted to be reversed even if the C-terminal donor residue and acceptor substrates are kept the same in the tested oligopeptides.

We proposed an explanation on how the mechanical forces acting on the nascent protein chain backbone quantitatively affect the rate of the

peptidyl transfer reaction. A pulling force exerted on the nascent chain backbone, directed from the PTC toward the exit tunnel, facilitates the peptide bond formation. The Eyring equation (3), determining the reaction rate constant where the Gibbs free energy transition barrier is explicitly modulated by the mechanical work of these forces, provides a tool to quantitatively predict the effects of the electrostatic forces on the time course of the peptide bond formation. In our approach, the mechanical work results from the dot product of the axial force with the curvilinear displacement. It is worth noticing that the mechanical work can, equivalently, be expressed as the dot product of a local electric dipole moment with the local electric field at the PTC, as was shown by other authors [48]. The physical value of the dipole moment is dependent on the type and charge of the amino acid being incorporated at the PTC. Whatever its origin, be it the dot product of a force with a displacement, or the dot product of a dipole moment with an electric field, the mechanical work modulates the Gibbs free energy barrier for the transition state. When the nascent chain threads through the tunnel and elongates toward the ribosome tunnel exit, the electrostatic potential profile along the full length of the tunnel impacts on the kinetics at the PTC. In this latter case, the mechanical work is best represented by the dot product of an axial force acting on the nascent oligopeptide embedded in the tunnel with the elongation displacement at the PTC.

4.1. Connections to previous studies

Free energy barriers for single positively charged amino acid like lysine (or negatively charged like aspartate) have been calculated in the work of Petrone et al. [22]. These authors found a significant free energy barrier along the main axis at the exit of the ribosome tunnel. The free energy barrier was measured in units of k_BT for lysine as $\sim 7\,k_BT$. For aspartate the barrier is smaller $\sim 2\,k_BT$. These authors also found that the barrier is much lower at the constriction site. Overall, the free energy barrier profile for a single positively charged amino acid lysine that they present in Fig. 3 (lower panel) is consistent with the electrostatic profile that we estimated from similar structural data of *Haloarcula marismortui* in our previous study [36].

The mechanical work modulating the activation energy of the peptide bond formation that we estimated in our current manuscript is the following:

- in case of a positively (or negatively) charged amino acid at the carboxy-terminal end of the peptidyl tRNA, the mechanical work is $\pm 5.3\text{pN}\cdot\text{nm}$, i.e. $= \pm 1.2 \times k_BT$ (at 37 Celsius degrees).
- in case of the 22-mer oligopeptide specific sequence described in our manuscript, the mechanical work is $\pm 0.86\text{pN}\cdot\text{nm}$, i.e. $= \pm 0.2 \times k_BT$ (at 37 Celsius degrees).

These mechanical work values are smaller than the local free energy barrier values calculated by Petrone et al. They are related to two different phenomena with different consequences. The free energy barriers calculated in Petrone et al. refer to a local intermolecular interaction of side chain amino acid residues (called individual chemical probes) with the wall or a local wall binding crevice along the exit tunnel, whereas the mechanical work values in our manuscript result from the global electrostatic interaction of charged probes in the nascent chain with the whole ribosome tunnel wall harboring negatively charged phosphates moieties. The former requires a Molecular Dynamics (MD) calculation of the so-called Potential of Mean Force (PMF) which includes non-bonded Van der Waals, London attraction, Pauli repulsion (Lennard-Jones potentials), Coulomb potential (without medium screening), non bonded hydrogen interaction and bonding harmonic interactions. The latter only includes electrostatic interaction calculated with the Yukawa-Debye-Hückel model (with attenuation due to medium electrostatic screening of mobile ions and solvent). The consequence of the electrostatic profile along the tunnel axis results in forces applied axially along the tunnel whereas the consequence of the free energy landscape as computed by MD simulations results in local attracting or repulsive forces orthogonal to the tunnel wall inner surface. Besides, the permittivity parameter values used in MD software tools to calculate the PMF are often the values of standard solvent and were not explicitly indicated in Petrone et al. paper. Comparing the two should be made with cautious.

In the abstract of their paper, Charneski et al. wrote that positively charged amino acids greatly retard ribosomes downstream from where they are encoded, consistent with the suggestion that positively charged residues interact with the negatively charged ribosomal exit tunnel [12]. The authors claim that: “Within transcripts, those regions with the highest ribosomal occupancy are those most likely to be just downstream of positively charged residues”. Their procedure clearly provides evidence that the charged amino acid slow down the ribosome on transcripts when the positively charged amino is engaged in the ribosome exit tunnel at a distance ranging between 3 and 15 codons upstream from their $x = 0$ reference position. It is not clear in the paper if the $x = 0$ reference position is the P-site or the A-site or other positional reference in the ribosome footprint range of 28 nucleotides (9-10 codons). The Material and Methods in the paper indicate that the ribosome footprint fragments data they used have not been mapped around the P or A-site or the active site of the peptidyl transferase center (PTC). Instead, the reference $x = 0$ only indicates the feature position of a codon coding for a single positively charged amino acid. Charneski et al. did not provide evidence that a positively charged amino acid at the C-terminal end of the peptidyl-tRNA would slow down the elongation cycle and thus increase ribosome density in ribosome profiling data. They provide evidence that positively charged amino acid already engaged in the ribosome exit tunnel slow down the elongation cycle. They also mentioned in their paper, that in some cases not slowing but speeding occurred and hence a decrease in ribosome density (result not shown).

Our results are not in contradiction with Charneski et al. results [12]. We actually have similar and overlapping conclusions. Two of our probing oligopeptides, the 22-mer and the 40-mer oligopeptides carry 3 and 5 positively charged amino acid at positions 18, 19, 20, or at positions 35, 36, 37, 38, 39 away from the P-site, respectively. For these two oligopeptide probes, we have predicted a slower rate in the peptide bond formation and hence in the elongation cycle (and hence an expected increased ribosome density footprint). It is only for our 10-mer oligoprobe carrying 3 charged amino acid at position 6, 7 and 8 away from the P-site that we predict a higher rate or a speeding up of the peptide bond formation. Even with this 10-mer, not being able to localize where the $x = 0$ reference is in Charneski et al. paper, with respect to the C-terminal amino acid at the peptidyl-tRNA (P-site), we cannot say that we have contradicting results. Unfortunately, Charneski et al. did not extend their analysis to negatively charged amino acids. Charneski et al. did not address the global shape or the complete profile of the electrostatic potential along the ribosome exit tunnel axis.

4.2. Assumptions, limitations and generalization

The electrostatic forces inside the ribosome exit tunnel are not the only contributing forces. Indeed, when the peptide chain has reached a certain length and its N-terminus has exited the tunnel, it is the structure of the chain itself (captured through the hydropathy) that determines its movement through the tunnel [5]. It should be added that the entropy driving forces upon protein folding outside the tunnel or tugging forces exerted from chaperone proteins could also contribute. Furthermore, the secondary structures which build already in the inner tunnel, harbor electric dipole moments interacting with the ambient electric field in the tunnel [49,50]. The ribosome exit tunnel is also known to be a protein-sensitive channel with gate-latch action and where sequence or specific side chain recognition regulate elongation [22]. These effects have not been considered in our theoretical study. We suggest however that any force, whatever its origin, acting on the backbone of the nascent chain will affect the rate constant of the peptide

bond formation. If the mechanical work of these forces can be quantitatively estimated, the impact on kinetics can also be quantitatively estimated through the Maxwell-Boltzmann factor that we have incorporated in the Eyring equation and in the Michaelis-Menten equation.

The oligopeptide probes of different lengths (10, 22 and 40-mer) for which we calculated the theoretical axial forces in this study are fully embedded in the tunnel and cannot make a complete path through the full length of the tunnel. Moreover, these oligopeptides are supposed to be unstructured (harboring no secondary structures). With these features, they are not concerned with the above limitations.

4.3. Output theoretical uncertainty calculated from the model input uncertainties and experimental uncertainty in the median time course measurements

The uncertainty in the calculated rates and median time course resulting from the model is larger than the experimental uncertainty resulting from the reaction rate experimental measurements using a quench flow apparatus as described in reference [24]. In the three designed pairs of oligopeptide probes with opposite charges (10-mer, 22-mer and 40-mer), the differences between the positively and the negatively charged probes in the median time courses are 13.4 ms, 17.70 ms, 10.80 ms respectively. For two of the three oligopeptide probes, the effect sizes are slightly larger than the sum of the associated theoretical uncertainties that were estimated in the last column of Table 1: $\Delta\tau_{1/2}^{\text{th.}} = 10.20\,\text{ms}\,(=4.3+5.9), 8.9\,\text{ms}\,(=5.3+3.6), 12.4\,\text{ms}\,(=7+5.4)$. The first two effect sizes in the difference between the median time courses for the 12-mer pair and the 22-mer pair of oligopeptides, are larger than the theoretical uncertainties resulting from the electrostatic model and the mechano-chemically modulated model of the peptide bond formation rate. Our main prediction is that we should observe a difference in time course measurements which is much larger than the experimental uncertainty ~ 3 ms. Refer to Figs. 2, 3 and 4 (f) where the expected differences are at least larger than 10.8 ms (one order of magnitude larger than the experimental uncertainty). Moreover, an important result of our contribution is that a reversal in the relative time course should be expected when comparing the 10-mer with the 22-mer oligopeptide probes with the given specific sequences of amino acid residues. This relative comparison has an expected effect size which is larger than the theoretical total uncertainty propagated in the model by the uncertainties in the input variables. The crucial salient feature of the model depends on the bell shape (inverse bell profile and presence of an electrostatic bump near the constriction site) of the electrostatic potential.

In our previously published references [36,42], we acknowledged the fact that the electrostatic potential exact profile can be species dependent. This is one of the reasons why we compared ribosomal structural x-ray crystallographic data across 5 different species. Other studies showed that it is indeed the case that the tunnel geometries can be different across the three domains of life [52]. However, there is a consensus regarding similar patterns across the three life kingdoms, in the shape of the profile along the central axis of the ribosome exit tunnel. Whatever the detailed profiles in the electrostatic potentials, there appears to be a common general pattern in the potential profiles and the qualitative predictions of our study should remain that the electrostatic interaction of the ribosome exit tunnel indeed contributes to the modulation of the peptide bond formation rate. It is expected, however, that the accuracy of the quantitative predictions is sensitive to the exact potential profile and is sensitive to its uncertainty.

4.4. Synthetic oligopeptides to be used as electrostatic probes and future perspectives

Our theoretical results applied to oligopeptides of variable lengths, which are long enough to probe the electrostatic environment inside the ribosome exit tunnel, should help the experimental design of real synthetic oligopeptides (translated from their synthetic transcripts by ribosomes *in vitro*) to experimentally test the validity of our predictions. These synthetic oligopeptides of different lengths and with charged residues specifically positioned at appropriate distances of the carboxyl-terminal end of the t-RNA at the P site, when puromycin is introduced as final acceptor substrate at the A-site, could be used as electrostatic probes of the electrostatic potential profile along the ribosome exit tunnel centerline.

In future studies, the Eyring equation and the modified Michaelis-Menten equation that we used can serve as quantitative tools to improve agent based models of protein synthesis by ribosomes such as the inhomogeneous totally asymmetric simple exclusion process. Specifically, the queueing time of the ribosome for the peptide bond formation (step 2) can be made quantitatively dependent on the charged amino acid residues distributed in the upstream nascent polypeptide, with a mobile window range of 30-70 residues, embedded in the ribosome exit tunnel.

The use of mechano-chemical kinetic models will facilitate the interpretation of optical tweezers experiments assessing the forces exerted on protein nascent chain in the ribosome exit tunnel or forces exerted by the ribosome on the mRNA molecule [13–15,43], as well as the interpretation of single mRNA molecule translation dynamics experiments [51].

We defer to future studies the application of the mechano-chemical kinetics model to improve the interpretation of Ribo-Seq data, ribosome occupancy maps of given transcripts and of the ribosome residence time on a given codon [6] as a function of the mRNA sequence upstream or downstream.

CRediT authorship contribution statement

Marc Joiret: Writing – review & editing, Writing – original draft, Visualization, Methodology, Formal analysis, Conceptualization. **Frederic Kerff:** Validation. **Francesca Rapino:** Conceptualization. **Pierre Close:** Conceptualization. **Liesbet Geris:** Writing – review & editing, Supervision, Resources, Investigation, Funding acquisition, Formal analysis, Conceptualization.

Declaration of competing interest

The authors declare that the research was conducted in the absence of any commercial or financial relationships that could be construed as a potential conflict of interest.

Acknowledgements

This work was supported by the FNRS-FWO EOS grant n^o30480119 (Join-t-against-Osteoarthritis), the FNRS-WELBIO-CR-2017S-02 (THERAtRAME) in Belgium and the European Research Council under the European Union's HORIZON EUROPE Framework Programme (HEU/20214-2027) /ERC grant agreement n^o1011088919 (INSTant-CARMA). The authors are grateful for the valuable contributions of the anonymous reviewers.

Appendix A

A.1. Uncertainty numerical estimation of the theoretical peptide bond formation rate using error propagation differential calculus

The classical error estimation of a multivariate function relies on the differential calculus and on the Leibniz derivative chain rule. The differential calculus provides an estimate of the maximum absolute uncertainty or the maximum relative uncertainty made on the numerical value of a function and is determined by the absolute uncertainties in the input variables. Let u be a function of multiple independent variables x, y, z, $\cdots$, t.

$$u = f(x, y, z, t) \tag{A-1}$$

Suppose that the numerical values of the input variables are known with their uncertainties Δx, Δy, Δz, $\cdots$, Δt. The numerical value of u will result with an uncertainty Δu

$$\Delta u = f(x + \Delta x,\ y + \Delta y,\ z + \Delta z,\ \cdots,\ t + \Delta t) - f(x, y, z, t). \tag{A-2}$$

To first order, if the input variables uncertainties are reasonably small, the total increase in u can be approximated by the total differential of u

$$\Delta u \approx \frac{\partial f}{\partial x}\Delta x + \frac{\partial f}{\partial y}\Delta y + \frac{\partial f}{\partial z}\Delta z + \cdots + \frac{\partial f}{\partial t}\Delta t. \tag{A-3}$$

Taking the absolute values of the errors (uncertainties) gives the inequality

$$|\Delta u| \leq \left|\frac{\partial f}{\partial x}\right| \cdot |\Delta x| + \left|\frac{\partial f}{\partial y}\right| \cdot |\Delta y| + \left|\frac{\partial f}{\partial z}\right| \cdot |\Delta z| + \cdots + \left|\frac{\partial f}{\partial t}\right| \cdot |\Delta t|. \tag{A-4}$$

It follows that upper limits can be estimated

$$|\Delta^* u| = \left|\frac{\partial f}{\partial x}\right| \cdot |\Delta^* x| + \left|\frac{\partial f}{\partial y}\right| \cdot |\Delta^* y| + \left|\frac{\partial f}{\partial z}\right| \cdot |\Delta^* z| + \cdots + \left|\frac{\partial f}{\partial t}\right| \cdot |\Delta^* t|. \tag{A-5}$$

Three classical results from this chain rule derivation are reminded

1. If $u = x + y + z$, then $|\Delta^* u| = |\Delta^* x| + |\Delta^* y| + |\Delta^* z|$.
2. If $u = x \cdot y$, then $|\Delta^* u| = |x| \cdot |\Delta^* y| + |y| \cdot |\Delta^* x|$.
3. If $u = \frac{x}{y}$, then $|\Delta^* u| = |\frac{1}{y}| \cdot |\Delta^* x| + |\frac{x}{y^2}| \cdot |\Delta^* y|$.

Applying this error calculus to the electrostatic potential profile model for $\Phi(z)$ and $E_z(z)$ that were derived in [36] (equations [3], [8], [19] and [20]), we can calculate an estimate in the uncertainty for the theoretical model of the electrostatic interaction in the ribosome exit tunnel. Namely, we can provide uncertainty estimates for the axial electric field E_z, the axial force, the mechanical work for a displacement along the ribosome exit tunnel central path (z displacement), and finally an uncertainty for the peptide bond reaction theoretical rate or its inverse, the median time course of the peptide bond formation.

The numerical values adopted for the uncertainties in the input variables resulted from complementary observational constraints. The atomic positions mapped on the tunnel surface, built from high precision x-ray solved structures of real ribosomes, set bounded ranges in the phenomenological constants σ and ϵ. These ranges are also constrained by the experimental electrostatic potential measurements that were made in the ribosome exit tunnel [40,41]. Altogether, these constraints jointly set the uncertainties order of magnitudes for the electrostatic model input variables. A close examination of the electrostatic profile showed in Fig. 1 suggests that different electrostatic potential profiles could accommodate the experimental confidence interval for the observed data points. All instances of alternative functions modeling the potential would have to be jointly consistent with the observed confidence intervals. This set limits in the lower and upper bounds in the space of values for the input variables of the electrostatic potential model. The numerical values and the uncertainties of the input variables that were used for the output uncertainty calculation are listed in Table 2.

Specifically, the experimental uncertainties for the potential show confidence interval values around $\simeq 5\,\mathrm{mV}$. This corresponds to an uncertainty of $\Delta\Phi(z) = \pm 2.5\,\mathrm{mV}$. The Yukawa-Debye Hückel model function for the electrostatic potential $\Phi(z)$ in equation (2) taking into account the water screening effect (26) in [36] requires that

$$\Delta\Phi \approx \left[\frac{R}{2\epsilon_0\epsilon_r} \cdot \Delta\sigma + \frac{\sigma \cdot R}{2} \cdot \frac{\epsilon_0 \Delta\epsilon_r}{\epsilon_0^2\epsilon_r^2} + \frac{\sigma}{2\epsilon_0\epsilon_r} \cdot \Delta R\right] \cdot e^{-\frac{\Delta}{\xi}} \tag{A-6}$$

This shows, for instance, that the uncertainties on Φ, σ, ϵ_r and R are jointly constrained by the model itself, i.e., by the Yukawa-Debye-Hückel laws of electrostatics in dielectric media. The numerical values listed in Table 2 comply with these constraints. The sequence of the uncertainty propagation is calculated as follows. The $E_z(z)$ electric field is a function of the minimal set of input variables $z, \sigma, \epsilon, R, L$.

$$E_z = f(z, \sigma, \epsilon, R, L) \tag{A-7}$$

The functions f are explicitly derived, for different ribosome exit tunnel geometries, in equations (3), (8), (19), (20) in [36]. To calculate an estimate of the uncertainty ΔE_z on the electric field E_z, we estimate from equation (3) in [36]

$$|\Delta^* E_z| = \left|\frac{\partial f}{\partial z}\right| \cdot |\Delta^* z| + \left|\frac{\partial f}{\partial \sigma}\right| \cdot |\Delta^* \sigma| + \left|\frac{\partial f}{\partial \epsilon_r}\right| \cdot |\Delta^* \epsilon_r| + \left|\frac{\partial f}{\partial R}\right| \cdot |\Delta^* R| + \left|\frac{\partial f}{\partial L}\right| \cdot |\Delta^* L| \tag{A-8}$$

Starting from the different geometries lead to more complicated formula but the order of magnitudes for the uncertainties are similar (not shown). The salient profile feature is the inverse bell shape of the potential. The first derivatives of the terms for the E_z uncertainty are:

$$\left|\frac{\partial f}{\partial z}\right| = \frac{\sigma R}{2\epsilon_0\epsilon_r}\left[-\frac{z+L}{(R^2+(z+L)^2)^{3/2}} + \frac{z}{(R^2+z^2)^{3/2}}\right] \tag{A-9}$$

$$\left|\frac{\partial f}{\partial \sigma}\right| = \frac{\sigma R}{2\epsilon_0\epsilon_r} \cdot \left(\frac{1}{\sqrt{R^2+(z+L)^2}} - \frac{1}{\sqrt{R^2+z^2}}\right) \tag{A-10}$$

$$\left|\frac{\partial f}{\partial \epsilon_r}\right| = \frac{\sigma R}{2\epsilon_0^2\epsilon_r^2} \cdot \left(\frac{1}{\sqrt{R^2+(z+L)^2}} - \frac{1}{\sqrt{R^2+z^2}}\right) \tag{A-11}$$

$$\left|\frac{\partial f}{\partial R}\right| = \frac{\sigma}{2\epsilon_0\epsilon_r} \cdot \left(\frac{1}{\sqrt{R^2+(z+L)^2}} - \frac{1}{\sqrt{R^2+z^2}}\right) + \frac{\sigma R^2}{2\epsilon_0\epsilon_r}\left[\frac{1}{(R^2+z^2)^{3/2}} - \frac{1}{(R^2+(z+L)^2)^{3/2}}\right]$$

$$\left|\frac{\partial f}{\partial L}\right| = \frac{\sigma R}{2\epsilon_0\epsilon_r} \cdot \frac{z+L}{(R^2+(z+L)^2)^{3/2}} \tag{A-12}$$

where, in all the above formulas, $\sigma = \sigma^* \cdot e^{-\frac{\Delta}{\xi}}$ to take into account the Gouy-Chapman screening length [36]. Using the numerical values listed in Table 2, the estimated maximum absolute uncertainty in E_z is numerically equal to $|\Delta^* E_z| \sim 170\,\mathrm{MV/cm}$ or $|\Delta^* E_z| \sim 0.3\,\mathrm{pN}/|e|$ when $z = -1.2\,\mathrm{nm}$.

The axial force uncertainty is the uncertainty of the electric field multiplied by the test charge. The uncertainty in the mechanical work W is obtained by applying the differential calculus in the same way.

$$W = q \cdot E_z \cdot dz \tag{A-13}$$

$$\Delta W = q \cdot dz \cdot \Delta E_z + q \cdot \Delta(dz) \cdot E_z. \tag{A-14}$$

The uncertainties on the reaction rate $k(F)$ in the presence of an axial force F and the median time course $\tau_{1/2}$ of the reaction are calculated as follows.

$$k(F) = k(0) \cdot e^{-\frac{W}{k_B T}} \tag{A-15}$$

$$\Delta k(F) = k(0) \cdot e^{-\frac{W}{k_B T}} \cdot \left(\frac{\Delta W}{k_B T}\right) + \Delta k(0) \cdot e^{-\frac{W}{k_B T}} \tag{A-16}$$

$$\tau_{1/2} = \frac{ln\,2}{k(F)} \tag{A-17}$$

$$\Delta\tau_{1/2} = ln\,2 \cdot \frac{\Delta k(F)}{k(F)^2}, \tag{A-18}$$

where $k_0 = 15.82\,\mathrm{s}^{-1}$ is the reference median reaction rate for neutral oligopeptide probes and $\Delta k_0 = 1.50\,\mathrm{s}^{-1}$ is the experimental uncertainty on experimental rate measurements, corresponding to an experimental uncertainty in the median time course of the peptide bond formation around $\sim 3\,\mathrm{ms}$, when puromycin is the A-site acceptor substrate. The output variables theoretical uncertainties are listed in Table 3 for three

Table 2
Numerical values and uncertainties of the electrostatic potential model input variables. The table rows list the model input variables σ, the surface charge density of the exit tunnel inner wall; ϵ_r, the dielectric response of the medium in the tunnel lumen; R, the tunnel radius; L, the tunnel length; z, the exact position in the tunnel where the potential and electric field are measured; Φ, the electrostatic potential.

input variable		units [-]	values	error	relative error	absolute error
unit charge	$q = \|e\|$	C	$1.602\,10^{-19}$			
surface charge density	σ	C/nm^2	$2.1\|e\|$	$\mathbf{\Delta}\sigma$	20%	$0.4\|e\|$
vacuum permittivity	$\epsilon_\mathbf{0}$	F/m	$8.85\,10^{-12}$			
relative permittivity (dielectric medium)	$\epsilon_\mathbf{r}$	–	78	$\mathbf{\Delta}\epsilon_\mathbf{r}$	70%	55
tunnel radius	$\mathbf{R}$	nm	0.5	$\mathbf{\Delta R}$	10%	0.05
tunnel length	$\mathbf{L}$	nm	10	$\mathbf{\Delta L}$	5%	0.5
position	$\mathbf{z}$	nm	−1.2	$\mathbf{\Delta z}$	25%	0.30
	$\mathbf{z}$	nm	−4.2	$\mathbf{\Delta z}$	25%	1.05
	$\mathbf{z}$	nm	−8.7	$\mathbf{\Delta z}$	25%	2.15
Gouy-Chapman screening length	ξ	nm	0.105			
charge attenuating factor (screening)	$e^{-\frac{\Delta}{\xi}}$	-	0.002			
electrostatic potential	$\mathbf{\Phi}$	mV	−15	$\mathbf{\Delta\Phi}$	17.5%	2.5

z are measured here from the exit tunnel entry port as origin. This corresponds to a shift by 8 nm from the z origin in Fig. 1.

Table 3
Numerical values and uncertainties of the electrostatic potential model and kinetics model output variables.

output variable		units [-]	values	uncertainty	absolute uncertainty
10-mer probe	$z \in [-8.95, -9.45]$ nm		$z_{\text{center}} = -1.2$ nm		
electric field	E_z	MV/cm		$\|\mathbf{\Delta}^* \mathbf{E_z}\|$	173
mechanical work	W	pN.nm	0.65	$\|\mathbf{\Delta}^* \mathbf{W}\|$	0.086
reaction rate	$k(F)$	s^{-1}			
fast		$\oplus$-mer	18.35	$\|\mathbf{\Delta}^* \mathbf{k}\|$	2.11
slow		$\ominus$-mer	13.61	$\|\mathbf{\Delta}^* \mathbf{k}\|$	1.56
median time course	$\tau^{th.}_{1/2}$	ms			
fast		$\oplus$-mer	37.6	$\|\mathbf{\Delta}^* \tau^{\mathbf{th.}}_{\mathbf{1/2}}\|$	4.3
slow		$\ominus$-mer	51	$\|\mathbf{\Delta}^* \tau^{\mathbf{th.}}_{\mathbf{1/2}}\|$	5.9
22-mer probe	$z \in [-11.95, -12.45]$ nm		$z_{\text{center}} = -4.2$ nm		
electric field	E_z	MV/cm		$\|\mathbf{\Delta}^* \mathbf{E_z}\|$	39
mechanical work	W	pN.nm	0.86	$\|\mathbf{\Delta}^* \mathbf{W}\|$	0.017
reaction rate	$k(F)$	s^{-1}			
slow		$\oplus$-mer	12.81	$\|\mathbf{\Delta}^* \mathbf{k}\|$	1.27
fast		$\ominus$-mer	19.30	$\|\mathbf{\Delta}^* \mathbf{k}\|$	1.91
median time course	$\tau^{th.}_{1/2}$	ms			
slow		$\oplus$-mer	53.5	$\|\mathbf{\Delta}^* \tau^{\mathbf{th.}}_{\mathbf{1/2}}\|$	5.3
fast		$\ominus$-mer	35.8	$\|\mathbf{\Delta}^* \tau^{\mathbf{th.}}_{\mathbf{1/2}}\|$	3.6
40-mer probe	$z \in [-16.2, -17.2]$ nm		$z_{\text{center}} = -8.7$ nm		
electric field	E_z	MV/cm		$\|\mathbf{\Delta}^* \mathbf{E_z}\|$	449
mechanical work	W	pN.nm	0.525	$\|\mathbf{\Delta}^* \mathbf{W}\|$	0.20
reaction rate	$k(F)$	s^{-1}			
slow		$\oplus$-mer	13.92	$\|\mathbf{\Delta}^* \mathbf{k}\|$	1.96
fast		$\ominus$-mer	17.88	$\|\mathbf{\Delta}^* \mathbf{k}\|$	2.51
median time course	$\tau^{th.}_{1/2}$	ms			
slow		$\oplus$-mer	49.5	$\|\mathbf{\Delta}^* \tau^{\mathbf{th.}}_{\mathbf{1/2}}\|$	7
fast		$\ominus$-mer	38.7	$\|\mathbf{\Delta}^* \tau^{\mathbf{th.}}_{\mathbf{1/2}}\|$	5.4

different regions in the ribosome exit tunnel. The calculations were conducted in the three regions of the tunnel spanned by the charged amino acid residues of the three designed oligopeptide pairs of probes.

References

[1] MacDonald CT, Gibbs JH, Pipkin AC. Kinetics of biopolymerization on nucleic acid templates. Biopolymers 1968;6:1.
[2] MacDonald CT, Gibbs JH. Concerning the kinetics of polypeptide synthesis on polyribosomes. Biopolymers 1969;7:707.
[3] von der Haar T. Mathematical and computational modelling of ribosomal movement and protein synthesis: an overview. Comput Struct Biotechnol J 2012;1:e201204002.
[4] Zur H, Tuller T. Predictive biophysical modeling and understanding of the dynamics of mRNA translation and its evolution. Nucleic Acids Res 2016;44:9031.
[5] Dao Duc K, Song Y. The impact of ribosomal interference, codon usage, and exit tunnel interactions on translation elongation rate variation. PLoS Genet 2018;14:e1007166.
[6] Dana A, Tuller T. The effect of tRNA levels on decoding times of mRNA codons. Nucleic Acids Res 2014;42:9171.
[7] Gorochowski T, Ignatova Z, Bovenberg R, Roubos H. Trade-offs between tRNA abundance and mRNA secondary structure support smoothing of translation elongation rate. Nucleic Acids Res 2015;43.
[8] Novoa EV, Pavon-Eternod M, Pan T, Ribas de Pouplana L. A role for tRNA modifications in genome structure and codon usage. Cell 2012;149(1):202.
[9] Lyu X, Yang Q, Li L, Dang Y, Zhou Z, Chen S, et al. Adaptation of codon usage to tRNA I34 modification controls translation kinetics and proteome landscape. PLoS Genet 2020;16.
[10] Sabi R, Tuller T. A comparative genomics study on the effect of individual amino acids on ribosome stalling. BMC Genomics 2015;16:S5.
[11] Requião RD, de Souza HJ, Rossetto S, Domitrovic T, Palhano FL. Increased ribosome density associated to positively charged residues is evident in ribosome profiling experiments performed in the absence of translation inhibitors. RNA Biol 2016;13:561.
[12] Charneski CA, Hurst LD. Positively charged residues are the major determinants of ribosomal velocity. PLoS Biol 2013;11:e1001508.
[13] Wen J-D, Lancaster L, Hodges HC, Zeri A, Yoshimura S, Noller H, et al. Following translation by single ribosomes one codon at a time. Nature (London) 2008;452:598.
[14] Liu T, Kaplan A, Alexander L, Yan S, Wen J-D, Lancaster L, et al. Direct measurement of the mechanical work during translocation by the ribosome. eLife 2014;3:e03406.
[15] Desai VP, Frank F, Lee A, Righini M, Lancaster L, Noller HF, et al. Co-temporal force and fluorescence measurements reveal a ribosomal gear shift mechanism of translation regulation by structured mRNAs. Mol Cell 2019;75:1007.
[16] Artieri CG, Fraser HB. Accounting for biases in riboprofiling data indicates a major role for proline in stalling translation. Genome Res 2014;24:2011.
[17] Pavlov MY, Watts RE, Tan Z, Cornish VW, Ehrenberg M, Forster AC. Slow peptide bond formation by proline and other N-alkylamino acids in translation. Proc Natl Acad Sci USA 2009;106(1):50.
[18] Shaw L, Zia R, Lee K. Totally asymmetric exclusion process with extended objects: a model for protein synthesis. Phys Rev E 2003;68:021910.
[19] Shah P, Ding Y, Niemczyk M, Kudla G, Plotkin JB. Rate-limiting steps in yeast protein translation. Cell 2013;153(7):1589.
[20] Raveh A, Margaliot M, Sontag ED, Tuller T. A model for competition for ribosomes in the cell. J R Soc Interface 2016;13(116).
[21] Greulich P, Ciandrini L, Allen R, Romano M. Mixed population of competing totally asymmetric simple exclusion processes with a shared reservoir of particles. Phys Rev E 2012;85:011142.
[22] Petrone PM, Snow CD, Del Lucent, Pande VJ. Side-chain recognition and gating in the ribosome exit tunnel. Proc Natl Acad Sci USA 2008;105:16549–54.
[23] Sharma PK, Xiang Y, Kato M, Warshel A. What are the roles of substrate-assisted catalysis and proximity effects in peptide bond formation by the ribosome? Biochemistry 2005;44(34):11307–14.
[24] Wohlgemuth I, Brenner S, Beringer M, Rodnina MV. Modulation of the rate of peptidyl transfer on the ribosome by the nature of substrates. J Biol Chem 2008;283:32229–34.

[25] Rodnina MV, Beringer M, Wintermeyer W. Mechanism of peptide bond formation on the ribosome. Q Rev Biophys 2006;39(3):203–25.
[26] Rodnina MV. Translation in prokaryotes. Cold Spring Harb Perspect Biol 2018;10(9).
[27] Beringer M, Rodnina MV. The ribosomal peptidyl transferase. Mol Cell 2007;26:311–21.
[28] Pape T, Wintermeyer W, Rodnina MV. Complete kinetic mechanism of elongation factor Tu-dependent binding of aminoacyl-tRNA to the A site of the E. coli ribosome. EMBO J 1998;17:7490–7.
[29] Sievers A, Beringer M, Rodnina MV, Wolfenden R. The ribosome as an entropy trap. Proc Natl Acad Sci USA 2004;101:7897–901.
[30] Schmeing TM, Huang KS, Kitchen DE, Strobel SA, Steitz TA. Structural insights into the roles of water and the 2' hydroxyl of the P site tRNA in the peptidyl transferase reaction. Mol Cell 2005;20:437–48.
[31] Trobro S, Åqvist J. Mechanism of peptide bond synthesis on the ribosome. Proc Natl Acad Sci USA 2005;102:12395–400.
[32] Trobro S, Åqvist J. Analysis of predictions for the catalytic mechanism of ribosomal peptidyl transfer. Biochemistry 2006;45(23):7049.
[33] Wallin G, Åqvist J. The transition state for peptide bond formation reveals the ribosome as a water trap. Proc Natl Acad Sci USA 2010;107(5):1888.
[34] Simonovic M, Steitz TA. A structural view on the mechanism of ribosome-catalyzed peptide bond formation. Biochim Biophys Acta 2009;1798:612–23.
[35] Polikanov YS, Steitz TA, Innis CA. A proton wire to couple aminoacyl-tRNA accommodation and peptide-bond formation on the ribosome. Nat Struct Mol Biol 2014;21(9):787–93.
[36] Joiret M, Kerff F, Rapino F, Close P, Geris L. Ribosome exit tunnel electrostatics. Phys Rev E 2022;105(1):1–43.
[37] Eyring H. The activated complex in chemical reactions. J Chem Phys 1935;3:107–15.
[38] Laidler KJ, King K. The development of transition state theory. J Phys Chem 1983;87:2657–64.
[39] Anslyn EV, Dougherty DA. Energy surfaces and kinetic analysis. In: Modern physical organic chemistry. Saucalito, CA, USA: University Science Books; 2005. p. 355–419.
[40] Lu J, Kobertz W, Deutsch C. Mapping the electrostatic potential within the ribosome exit tunnel. J Mol Biol 2007;371:1378–91.
[41] Lu J, Deutsch C. Electrostatics in the ribosomal tunnel modulate chain elongation rates. J Mol Biol 2008;384:73–86.
[42] Joiret M, Rapino F, Close P, Geris L. A simple geometrical model of the electrostatic environment around the catalytic center of the ribosome and its significance on the elongation cycle. Comput Struct Biotechnol J 2023;21:3768–95.
[43] Kaiser Christian, Tinoco Ignacio. Probing the mechanisms of translation with force. Chem Rev 2014;114:3266.
[44] Bell GI. Models for the specific adhesion of cells to cells. Science 1978;200:618–27.
[45] Bustamante C, Chemla YR, Forde NR, Izhaky D. Mechanical processes in biochemistry. Annu Rev Biochem 2004;73:705–48.
[46] Ribas-Arino J, Marx D. Covalent mechanochemistry: theoretical concepts and computational tools with applications to molecular nanomechanics. Chem Rev 2012;112:5412–87.
[47] Deutsch C. Tunnel vision: insights from biochemical and biophysical studies. In: Ito K, editor. Regulatory nascent polypeptides. Tokyo: Springer; 2014. p. 61–86.
[48] Fried SD, Boxer SG. Electric fields and enzyme catalysis. Annu Rev Biochem 2017;86:387–415.
[49] Mercier E, Rodnina M. Co-translational folding trajectory of the HEMK helical domain. Biochemistry 2020;57:3460.
[50] Liutkute M, Maiti M, Samatova E, Enderlein J, Rodnina MV. Gradual compaction of the nascent peptide during cotranslational folding on the ribosome. eLife 2020;9:e60895.
[51] Morisaki T, Lyon K, DeLuca KF, DeLuca JG, English BP, Zhang Z, et al. Real-time quantification of single RNA translation dynamics in living cells. Science 2016;352:1425.
[52] Dao Duc K, Batra SS, Bhattacharya N, Cate JHD, Song Y. Differences in the path to exit the ribosome across the three domains of life. Nucleic Acids Res 2019;47(8):4198–210.